Supplementary Information for

Efficient Thin-Film Perovskite Solar Cells from a Two-Step Sintering of Nanocrystals

Yuhao Peng[†,‡], *Junli Huang*[†,‡], *Lue Zhou*[†,‡], *Yuncheng Mu*[†], *Shuyao Han*[†], *Shu Zhou*[†,*], *Pingqi Gao*[†,*]

[†] *School of Materials, Sun Yat-sen University, Guangzhou 510275, China*

[‡] *These authors contribute equally.*

E-mail: **zhoush67@mail.sysu.edu.cn*

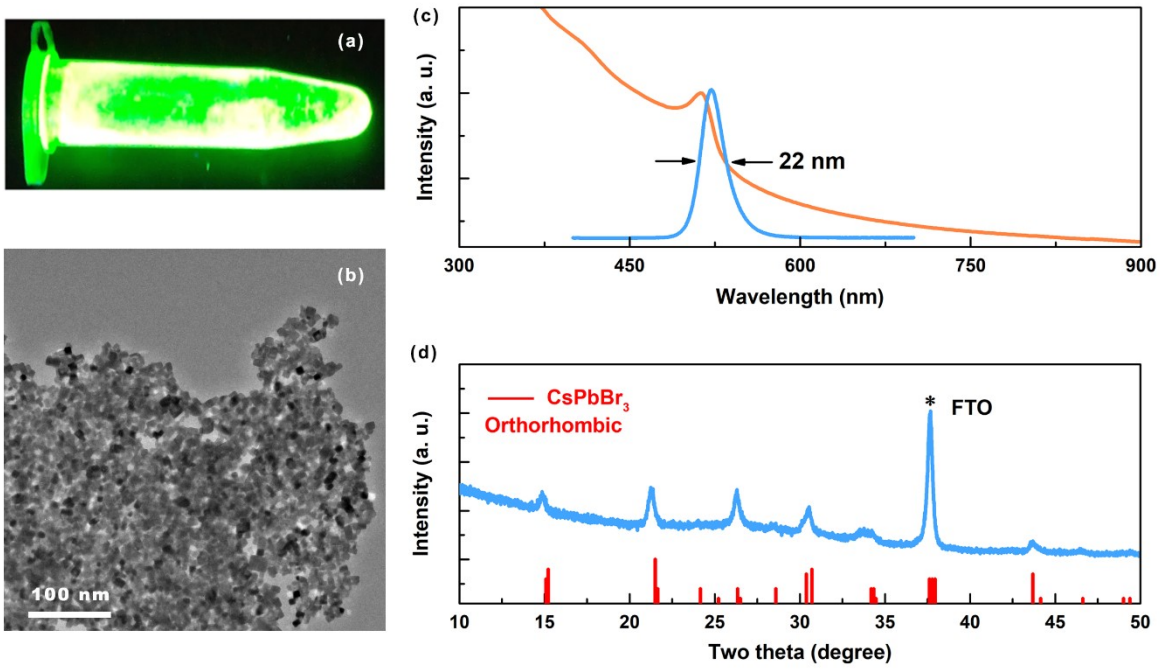

Figure S1. Strongly-emissive $CsPbBr_3$ NCs. (a) Image of a colloidal $CsPbBr_3$-NC ink under UV light. (b) Low-resolution TEM image of $CsPbBr_3$ NCs. (b) Optical absorption and PL spectra of $CsPbBr_3$ NCs. (c) XRD result of $CsPbBr_3$ NCs indicating an orthorhombic crystal lattice.

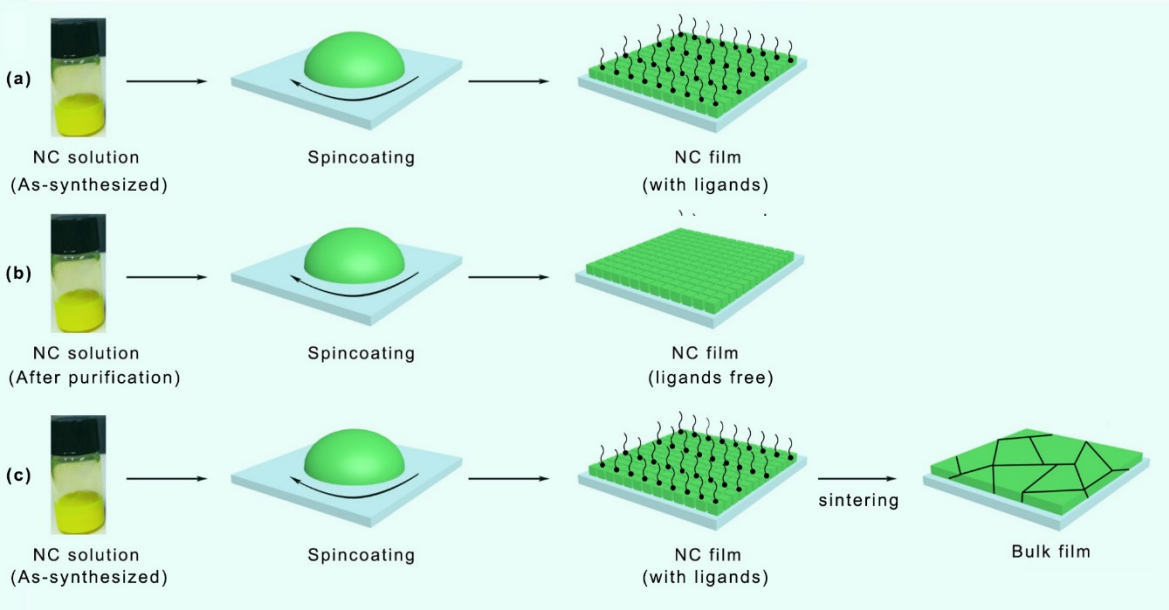

Figure S2. Schematic showing deposition of $CsPbBr_3$ films from NC inks. (a) As-synthesized $CsPbBr_3$ NCs are directly spincoated onto a FTO substrate, resulting in NC film with short alky ligands (b) $CsPbBr_3$ NCs are purified by washing in toluene for two times before spincoating, resulting in NC film that are free of ligands. (c) As-synthesized $CsPbBr_3$ NCs are spincoated onto a FTO substrate followed by sintering, resulting in bulk film. The process can then be repeated to create a perovskite film with desired thickness.

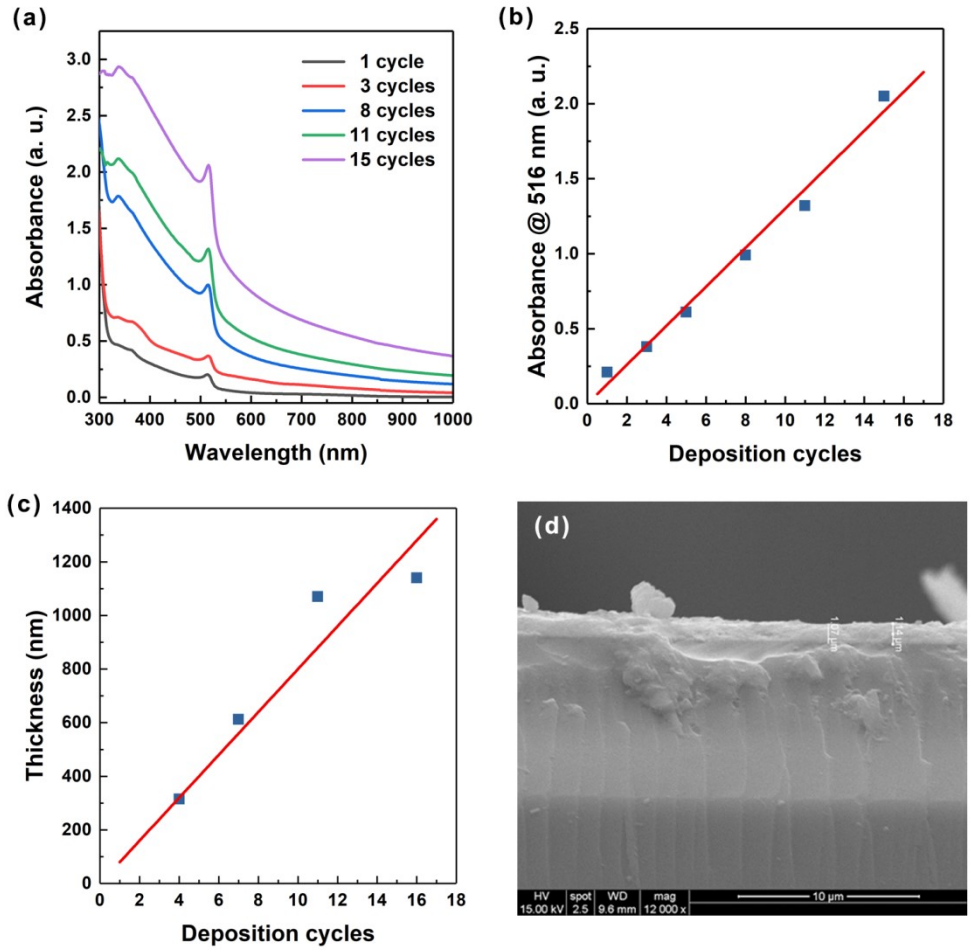

Figure S3. (a) Absorption spectra of $CsPbBr_3$ NC films, depending on the number of NC deposition cycles. (b) Normalized absorption at 516 nm for $CsPbBr_3$ NC films. (c) Thickness of $CsPbBr_3$ NC films measured by SEM, depending on the number of NC deposition cycles. (d) SEM image of a $CsPbBr_3$ NC film on a FTO glass substrate.

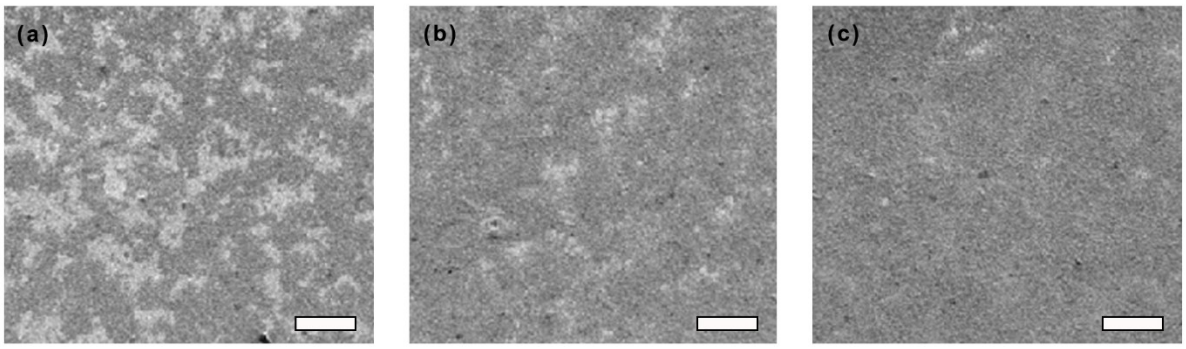

Figure S4. SEM images of $CsPbBr_3$-NC films show coverage of the substrate depending on the number of NC deposition cycles. (a) One-cycle, (b) two-cycle and (c) three-cycle spin-coating. The scale bar for all iamges is 10 μm.

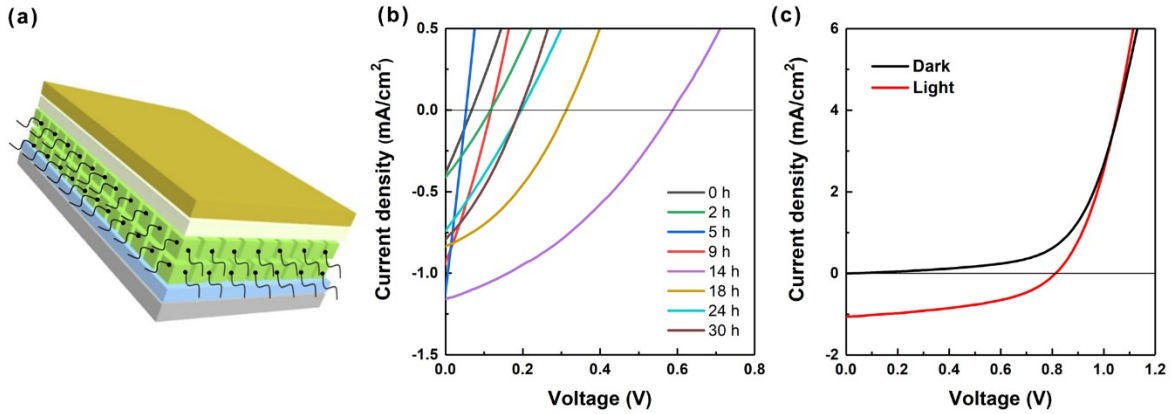

Figure S5. (a) Schematic showing the solar cell device structure. The $CsPbBr_3$ NCs are surface terminated with short ligands. (b) Current density-voltage curves of the solar cells as a function of the oxidation time of Spiro-MeoTAD in dry air. (c) Current density-voltage curves of the solar cells measured under dark and light (AM 1.5) conditions.

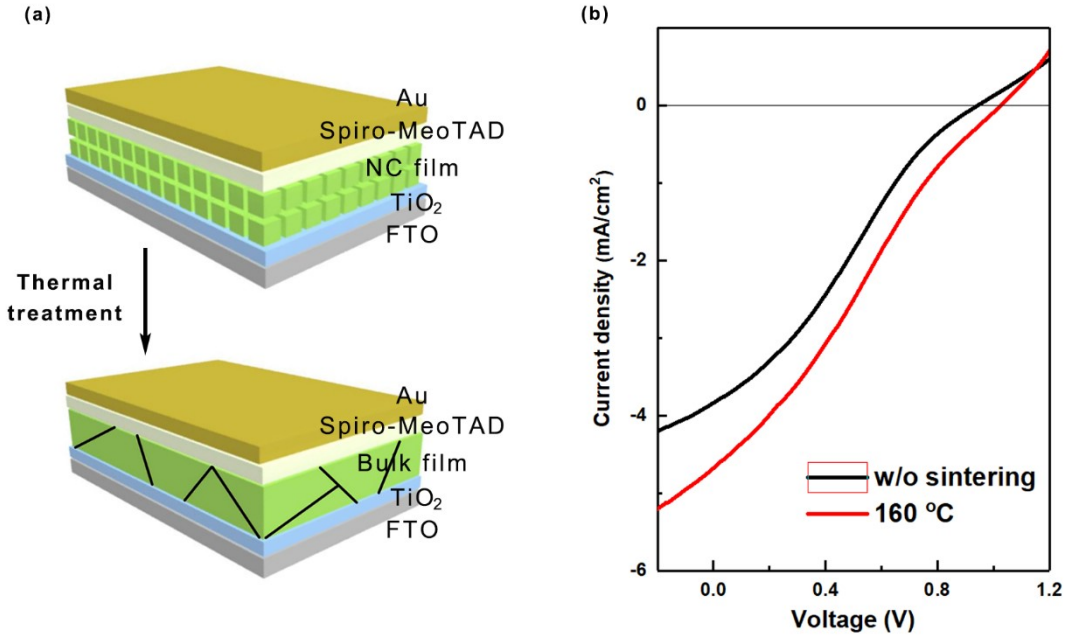

Figure S6. Effect of sintering on the performance of solar cells based on purified $CsPbBr_3$ NCs.

Table S1. Performance of the $CsPbBr_3$ solar cells as a function of the deposition cycles.

Method	Deposition cycles	V_{oc} (V)	J_{sc} (mA/cm^2)	FF	PCE (%)
As-synthesized	3	0.64	0.90	0.35	0.20
	6	0.59	0.80	0.40	0.19
	9	0.62	0.95	0.37	0.22
	12	0.55	0.91	0.40	0.20
Purified	6	0.94	2.84	0.24	0.64
	9	1.02	6.26	0.31	1.97
Sintered	6	0.85	5.70	0.51	2.47
	9	1.05	6.76	0.52	3.71
	12	1.08	5.35	0.42	2.42
	15	1.09	4.30	0.42	1.96

Table S2. Performance of the $CsPbBr_3$ solar cells as a function of the sintering temperature.

Temperature	V_{oc} (V)	J_{sc} (mA/cm^2)	FF	PCE (%)
w/o sintering	0.60±0.04	0.89±0.06	0.38±0.02	0.20±0.01
90 °C	1.35±0.02	0.92±0.05	0.49±0.02	0.62±0.04
160 °C	1.16±0.03	2.14±0.26	0.35±0.03	0.86±0.12
230 °C	1.23±0.03	6.44±0.56	0.50±0.04	3.90±0.37
280 °C	1.28±0.03	5.85±0.28	0.38±0.10	2.88±0.83

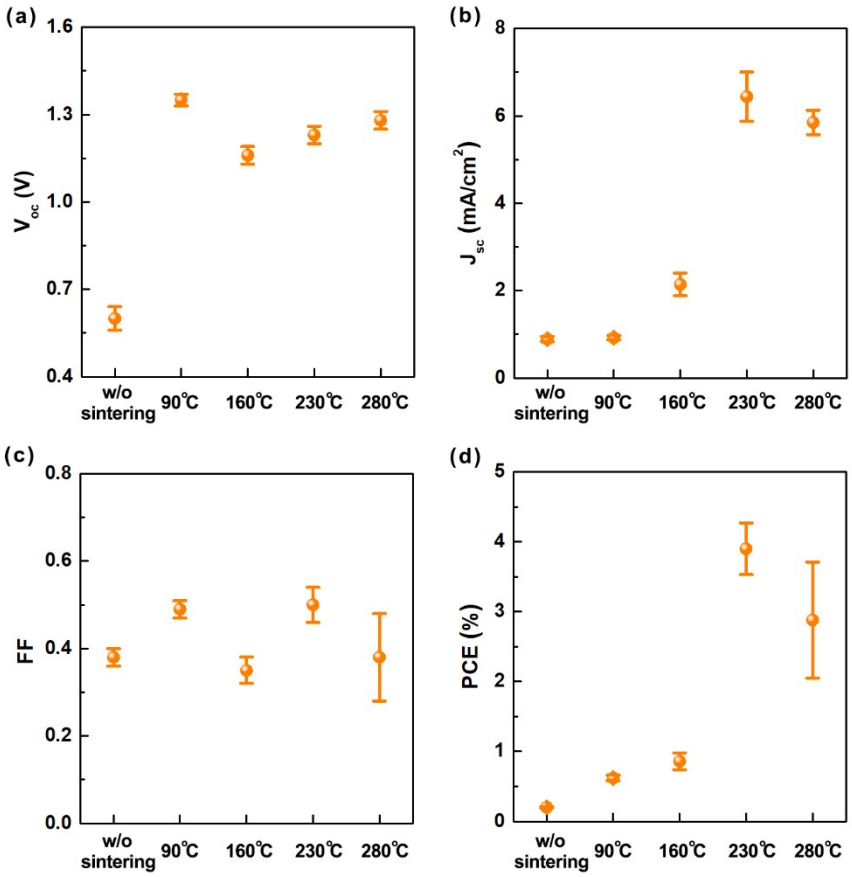

Figure S7. Device performance of the $CsPbBr_3$ solar cells as a function of the sintering temperature. Each point represents 9 contacts from the same film. (a) V_{oc}. (b) J_{sc}. (c) FF. (d) PCE.

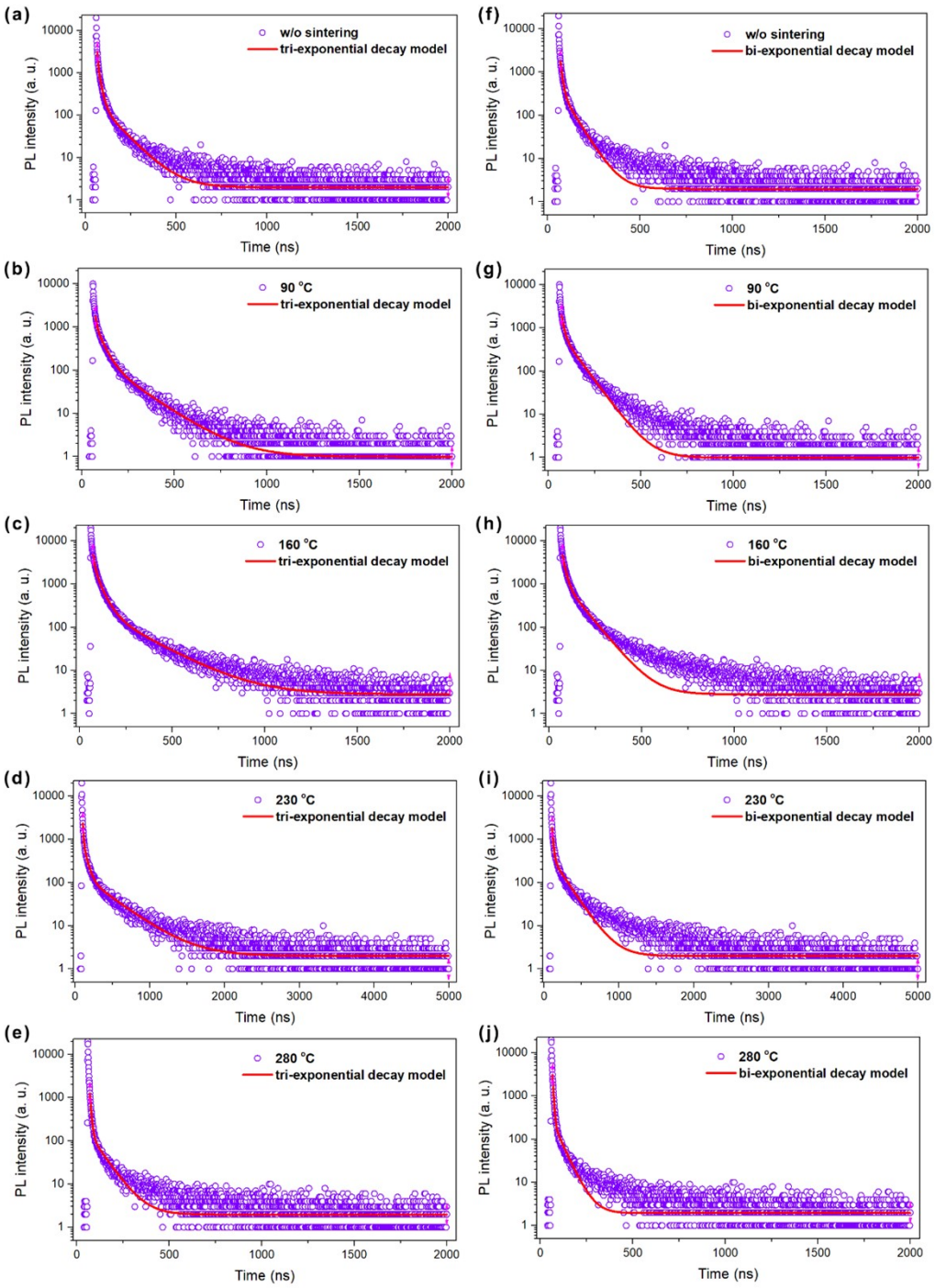

Figure S8. Fitting of the TRPL data by (a-e) a tri-exponential decay model and (f-j) a bi-exponential decay model, respectively. It is found that the curves could be better fitted by a tri-exponential decay model than a bi-exponential decay model. Therefore, a tri-exponential decay model was employed to fit all the curves in this work.

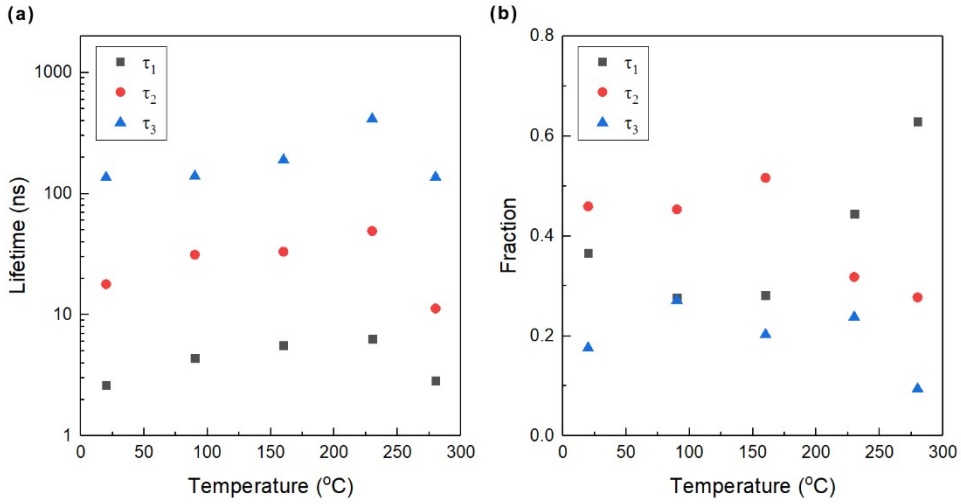

Figure S9. The TRPL curves are fitted with a three-component exponential decay. The decay lifetime (τ_1, τ_2, τ_3,) and corresponding fraction (B_1, B_2, B_3) are obtained. The average lifetime (τ_{ave}) is related to the lifetime and fraction of each decay component as $\tau_{ave} = \frac{B_1\tau_1^2 + B_2\tau_2^2 + B_3\tau_3^2}{B_1\tau_1 + B_2\tau_2 + B_3\tau_3}$.

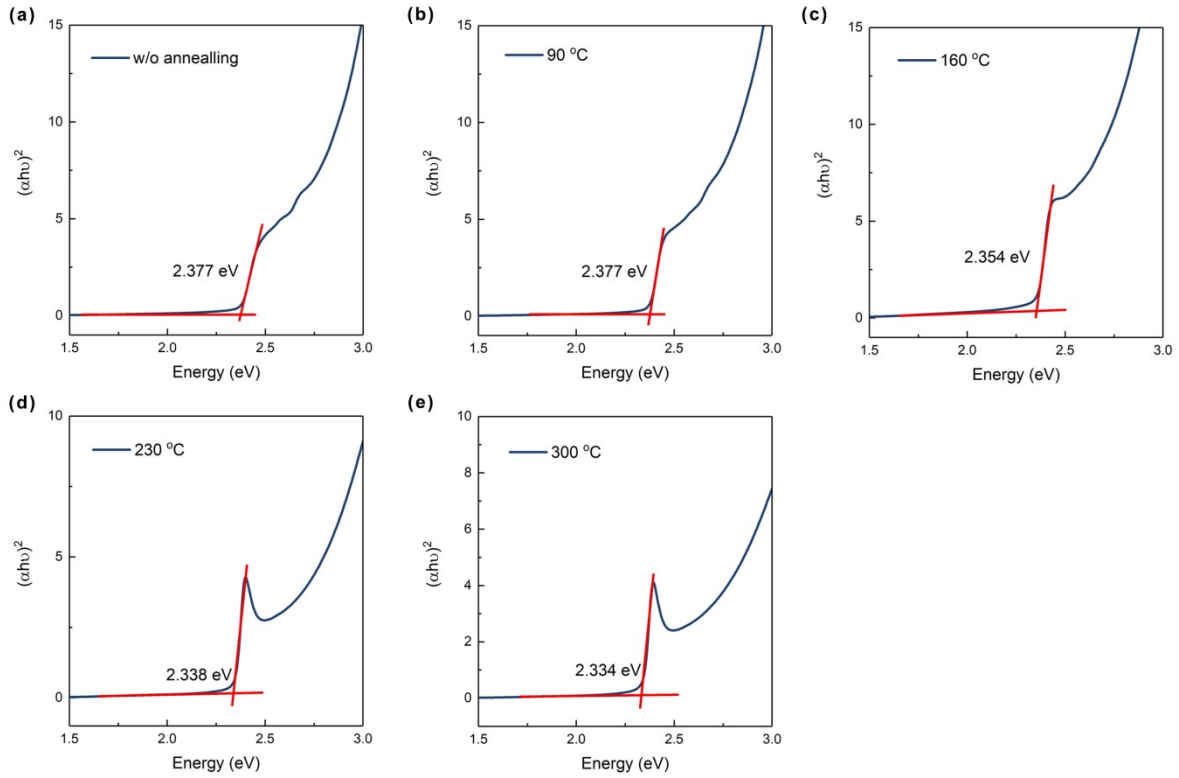

Figure S10. Tauc plot of absorption spectra of $CsPbBr_3$-NC films after annealing at different temperatures.

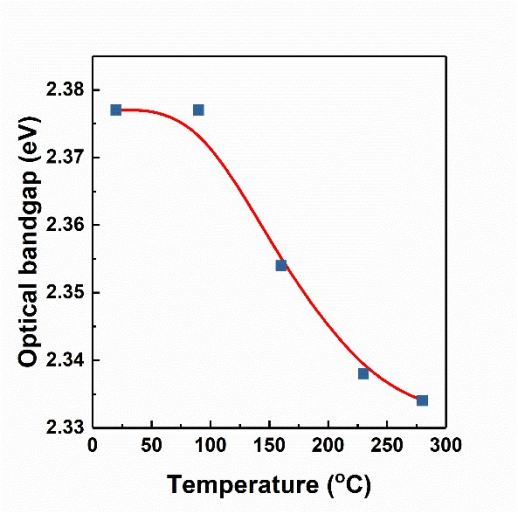

Figure S11. Evolution of optical bandgap of $CsPbBr_3$ NC films with increasing annealing temperature. When the T increases to 100 °C, the E_g remains almost unchanged, suggesting the size of NCs remains unchanged. As the T further increases, the E_g gradually decreases. The trend of E_g shift is consistent with the increase of grain size after thermal sintering.

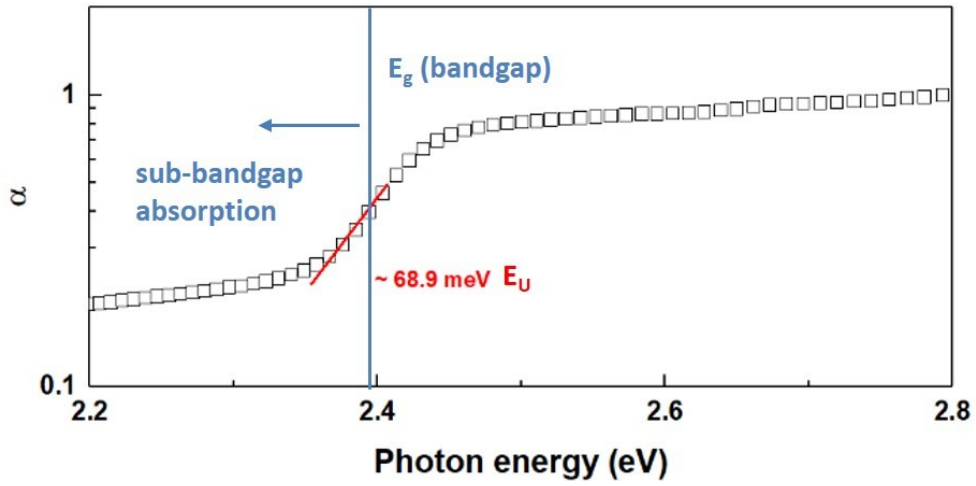

Figure S12. Calculation of E_U from fitting of sub-bandgap absorption by Equation 1.

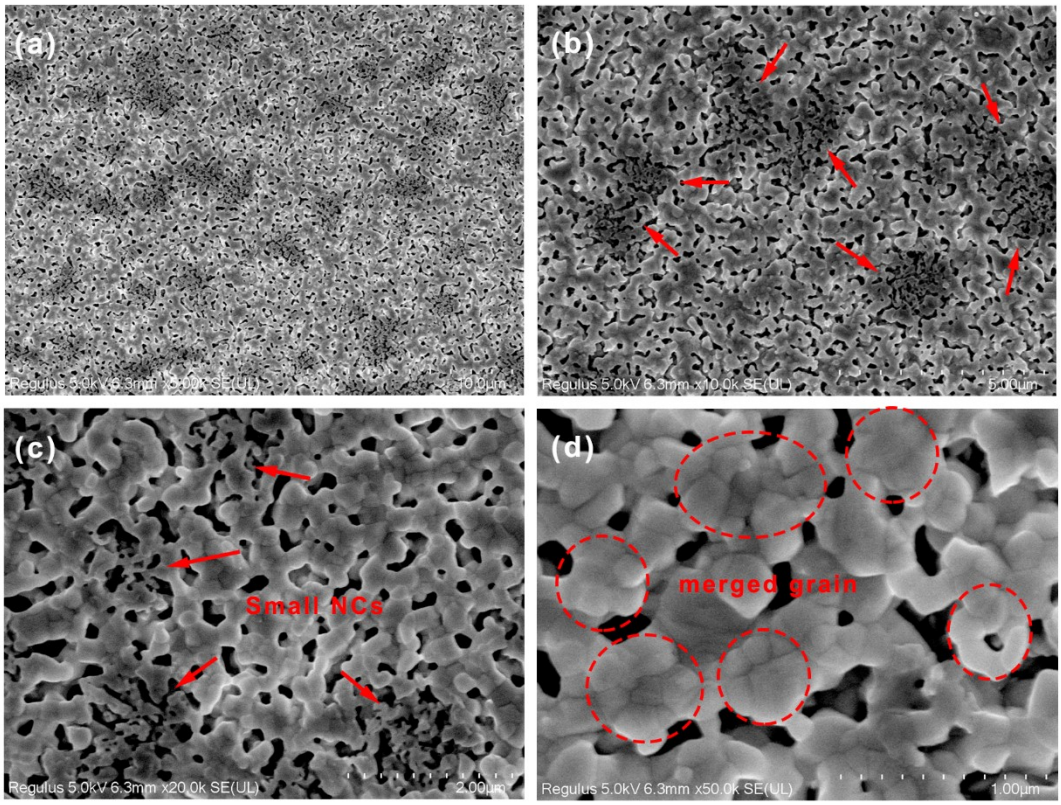

Figure S13. SEM images of the $CsPbBr_3$ film after sintering at 160 ºC taken at different magnifications. Both small NCs and merged grains can be observed in this intermediate stage. In the absence of reaction precursors, material migrates from smaller NCs to larger grains in a defocusing process analogous to Ostwald ripening observed normally in fabrication process.

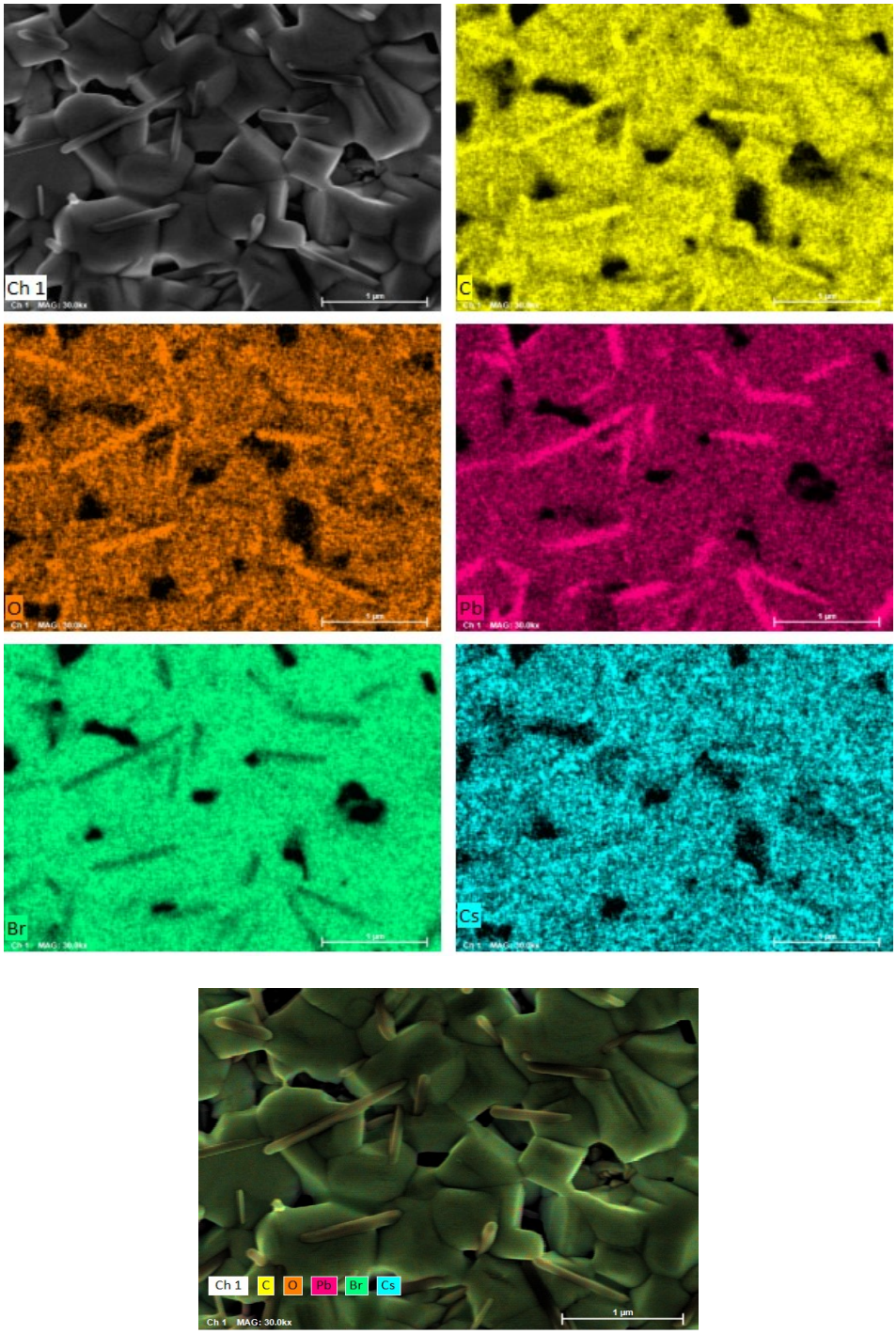

Figure S14. EDX mapping of the $CsPbBr_3$ film after sintering at 280 ºC. The new grains with a rod shape were identified to be $PbCO_3$ from the C, O and Pb spectrum.

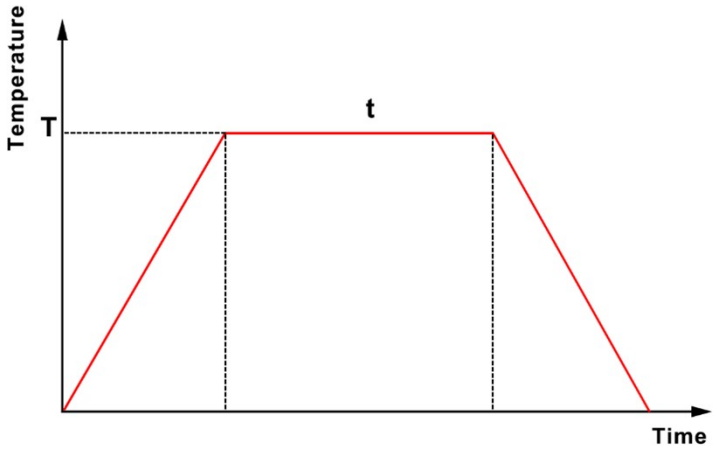

Figure S15. Illustrative representation of the one-step sintering plot. All the samples were heated from room temperature at a heating rate of 30 °C/min.

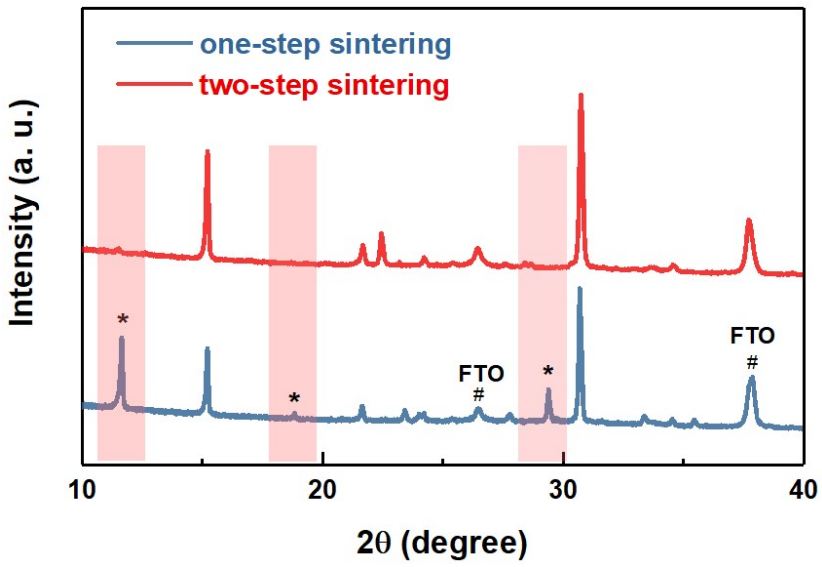

Figure S16. XRD patterns for the $CsPbBr_3$ films obtained by one-step sintering (280 °C 2h) and two-step sintering (230 °C 2h + 280 °C 20 min).

Table S3. Performance of the $CsPbBr_3$ solar cells obtained by one-step sintering and two-step sintering.

Method		V_{oc} (V)	J_{sc} (mA/cm^2)	FF	PCE (%)
One-step sintering (230 ^{o}C 2h)	Forward	1.24	6.75	0.49	4.07
	Backward	1.29	6.55	0.39	3.29
One-step sintering (280 ^{o}C 2h)	Forward	1.05	6.44	0.52	3.53
	Backward	0.99	6.52	0.34	2.18
Two-step sintering (230 ^{o}C 2h + 280 ^{o}C 20 min)	Forward	1.35	7.18	0.54	5.23
	Backward	1.33	6.92	0.51	4.71

Table S4. Performance of $CsPbBr_3$-based planar perovskite solar cells.

Device configuration	Method	V_{oc} (V)	J_{sc} (mA/cm^2)	FF	PCE (%)	Reference
FTO/c-TiO_2/$CsPbBr_3$/Spiro/Au	Spin-coating	0.96	6.76	0.73	4.7	[1]
FTO/c-TiO_2/$CsPbBr_3$/PTAA/Au	Spin-coating	1.28	6.24	0.74	5.9	[1]
FTO/c-TiO_2/$CsPbBr_3$/Spiro/Au	Spin-coating	1.41	7.05	0.55	5.5	[2]
FTO/c-TiO_2/$CsPbBr_3$/Spiro/Au	Spin-coating	1.54	5.65	0.62	5.4	[3]
FTO/c-TiO_2/$CsPbBr_3$/Spiro/Au	Evaporation	1.27	6.45	0.77	6.4	[4]
FTO/c-TiO_2/$CsPbBr_3$/Spiro/Au	Sintering	1.35	7.18	0.54	5.2	This work
FTO/GQDs/$CsPbBr_3$/PQDs/carbon	Spin-coating	1.21	5.08	0.66	4.1	[5]
FTO/ c-TiO2/$CsPbBr_3$/P3HT:PCBM/carbon	Spin-coating	1.5	7.82	0.76	8.9	[6]
FTO/ c-TiO_2/$CsPbBr_3$/ $CuCrO_2$ NCs /carbon	Spin-coating	1.63	7.73	0.86	10.9	[7]
FTO/ c-TiO_2/$CsPbBr_3$/ $CuInS_2$:ZnS QDs /carbon	Spin-coating	1.62	7.81	0.85	10.8	[8]
FTO/c-TiO_2/ZrO_2/$CsPbBr_3$/carbon	Screen-printing	1.36	7.21	0.58	5.7	[9]
FTO/c-TiO_2/$CsPbBr_3$/CuPc/carbon	Evaporation	1.33	7.59	0.75	7.6	[10]

Reference

(1) Kulbak, M.; Cahen, D.; Hodes, G. How Important Is the Organic Part of Lead Halide Perovskite Photovoltaic Cells? Efficient CsPbBr3 Cells. *The Journal of Physical Chemistry Letters* **2015**, *6*, 2452-2456.

(2) Hoffman, J. B.; Zaiats, G.; Wappes, I.; Kamat, P. V. CsPbBr3 Solar Cells: Controlled Film Growth through Layer-by-Layer Quantum Dot Deposition. *Chemistry of Materials* **2017**, *29*, 9767-9774.

(3) Akkerman, Q. A.; Gandini, M.; Di Stasio, F.; Rastogi, P.; Palazon, F.; Bertoni, G.; Ball, J. M.; Prato, M.; Petrozza, A.; Manna, L. Strongly emissive perovskite nanocrystal inks for high-voltage solar cells. *Nature Energy* **2016**, *2*, 16194.

(4) Lei, J.; Gao, F.; Wang, H.; Li, J.; Jiang, J.; Wu, X.; Gao, R.; Yang, Z.; Liu, S. Efficient planar CsPbBr3 perovskite solar cells by dual-source vacuum evaporation. *Solar Energy Materials and Solar Cells* **2018**, *187*, 1-8.

(5) Duan, J.; Zhao, Y.; He, B.; Tang, Q. Simplified Perovskite Solar Cell with 4.1% Efficiency Employing Inorganic CsPbBr3 as Light Absorber. *Small* **2018**, *14*, 1704443.

(6) Du, J.; Duan, J.; Duan, Y.; Tang, Q. Tailoring organic bulk-heterojunction for charge extraction and spectral absorption in CsPbBr3 perovskite solar cells. *Science China Materials* **2021**, *64*, 798-807.

(7) Duan, J.; Wang, Y.; Yang, X.; Tang, Q. Alkyl-Chain-Regulated Charge Transfer in Fluorescent Inorganic CsPbBr3 Perovskite Solar Cells. *Angewandte Chemie International Edition* **2020**, *59*, 4391-4395.

(8) Duan, J.; Zhao, Y.; Wang, Y.; Yang, X.; Tang, Q. Hole-Boosted Cu(Cr,M)O2 Nanocrystals for All-Inorganic CsPbBr3 Perovskite Solar Cells. *Angewandte Chemie International Edition* **2019**, *58*, 16147-16151.

(9) Poli, I.; Baker, J.; McGettrick, J.; De Rossi, F.; Eslava, S.; Watson, T.; Cameron, P. J. Screen printed carbon CsPbBr3 solar cells with high open-circuit photovoltage. *Journal of Materials Chemistry A* **2018**, *6*, 18677-18686.

(10) Liu, X.; Tan, X.; Liu, Z.; Sun, B.; Li, J.; Xi, S.; Shi, T.; Liao, G. Sequentially vacuum evaporated high-quality CsPbBr3 films for efficient carbon-based planar heterojunction perovskite solar cells. *Journal of Power Sources* **2019**, *443*, 227269.

(1) Kulbak, M.; Cahen, D.; Hodes, G. How Important Is the Organic Part of Lead Halide Perovskite Photovoltaic Cells? Efficient $CsPbBr_3$ Cells. *The Journal of Physical Chemistry Letters* **2015**, *6*, 2452-2456.

(2) Hoffman, J. B.; Zaiats, G.; Wappes, I.; Kamat, P. V. $CsPbBr_3$ Solar Cells: Controlled Film Growth through Layer-by-Layer Quantum Dot Deposition. *Chemistry of Materials* **2017**, *29*, 9767-9774.

(3) Akkerman, Q. A.; Gandini, M.; Di Stasio, F.; Rastogi, P.; Palazon, F.; Bertoni, G.; Ball, J. M.; Prato, M.; Petrozza, A.; Manna, L. Strongly emissive perovskite nanocrystal inks for high-voltage solar cells. *Nature Energy* **2016**, *2*, 16194.

(4) Lei, J.; Gao, F.; Wang, H.; Li, J.; Jiang, J.; Wu, X.; Gao, R.; Yang, Z.; Liu, S. Efficient planar $CsPbBr_3$ perovskite solar cells by dual-source vacuum evaporation. *Solar Energy Materials and Solar Cells* **2018**, *187*, 1-8.

(5) Duan, J.; Zhao, Y.; He, B.; Tang, Q. Simplified Perovskite Solar Cell with 4.1% Efficiency Employing Inorganic $CsPbBr_3$ as Light Absorber. *Small* **2018**, *14*, 1704443.

(6) Du, J.; Duan, J.; Duan, Y.; Tang, Q. Tailoring organic bulk-heterojunction for charge extraction and spectral absorption in $CsPbBr_3$ perovskite solar cells. *Science China Materials* **2021**, *64*, 798-807.

(7) Duan, J.; Wang, Y.; Yang, X.; Tang, Q. Alkyl-Chain-Regulated Charge Transfer in Fluorescent Inorganic $CsPbBr_3$ Perovskite Solar Cells. *Angewandte Chemie International Edition* **2020**, *59*, 4391-4395.

(8) Duan, J.; Zhao, Y.; Wang, Y.; Yang, X.; Tang, Q. Hole-Boosted $Cu(Cr,M)O_2$ Nanocrystals for All-Inorganic $CsPbBr_3$ Perovskite Solar Cells. *Angewandte Chemie International Edition* **2019**, *58*, 16147-16151.

(9) Poli, I.; Baker, J.; McGettrick, J.; De Rossi, F.; Eslava, S.; Watson, T.; Cameron, P. J. Screen printed

carbon $CsPbBr_3$ solar cells with high open-circuit photovoltage. *Journal of Materials Chemistry A* **2018**, *6*, 18677-18686.

(10) Liu, X.; Tan, X.; Liu, Z.; Sun, B.; Li, J.; Xi, S.; Shi, T.; Liao, G. Sequentially vacuum evaporated high-quality $CsPbBr_3$ films for efficient carbon-based planar heterojunction perovskite solar cells. *Journal of Power Sources* **2019**, *443*, 227269.